Fawzy *et al.*
Journal of Engineering and Applied Science (2022) 69:82
https://doi.org/10.1186/s44147-022-00115-2

Journal of Engineering and Applied Science

RESEARCH Open Access

Seismic performance of cable-stayed bridges with different geometric conditions

Ahmed M. Fawzy*, Khaled F. El-Kashif and Hany A. Abdalla

*Correspondence: ahmedfawzy9596@yahoo.com

Structural Engineering Department, Cairo University, Giza 12613, Egypt

Abstract

Cable-stayed bridges have gained greater coverage in the last few decades. This study focuses mainly on two parameters. Firstly, the shape of pylons; the performance of many shapes is investigated after being exposed to an earthquake. Secondly, the effect of changing deck width of an inverted Y-shaped pylon with variation in main span length. The numerical study was performed using MIDAS civil software. It was concluded that the most efficient pylon shape in terms of seismic performance was that of pyramid shape followed by a delta shape. In addition, it was found that changing deck width for the same main span gives a negligible difference to normalized shear force.

Keywords: Cable-stayed bridges, Pylon shapes, Response spectrum, Deck-tower interaction, Deck width

Introduction

Cable-stayed bridges are indeterminate structures. There are three major subsystems in the structural system of cable-stayed bridges: girder (deck), tower (pylon), and cables. The relationship between those subsystems makes cable-stayed bridges structurally efficient for long spans [28]. Cable-stayed bridges for the span ranges of 700–1500m have been proved to be mechanically, cost-effectively, and aerodynamically superior to suspension bridges [23]. However, the high-straining actions due to seismic loads may cause structural damage if the analysis does not correctly investigate such loads.

Dischinger F. has established the need to raise cable stress in order to minimize the sag effect. This advance gave the first spark of the beginning of a system that mainly depends on cables. It should be noted that cable-stayed bridges can now be analyzed with a high level of precision using high-speed digital computers and advanced analytical methods [21]. Cable-stayed bridges currently extend over distances from 200 to 1000 m, like the Russky Bridge of 1104 m in Russia and the Sutong Bridge of 1088 m in China [38]. Some designers took the view that a cable-stayed bridge is a linear structure with cables serving as linear tension members [18]. In fact, the cables show nonlinear behavior as a result of their own weights changing the tension in the cables. If we ignore the sag effect in the static analysis, an error of up to 15% may occur [21]. Other studies consider the non-linearity of cables that results from the sagging effect of different approaches. A study by Fabrizio Greco, Paolo Lonetti, and Arturo Pascuzzo was

concerned with the dynamic behavior of cable-stayed bridges subjected to moving loads and affected by an accidental failure in the cable suspension system [13]. The first order by the Taylor expansion in terms of the incremental cable stress distribution, by means of a linearized equation, is the approach that was followed in their study. These equations were based on a vector containing the displacements and subjected to the stress distribution in cable, loading parameter. P. Lonetti and A. Pascuzzo investigated damage and failure behavior on the cable system in their study, which can be used to predict the response of hybrid cable-stayed suspension bridges subjected to moving loads [24, 25]. To consider the non-linearity of cables, they adopted Multi Element Cable System (MECS) approach. This approach discretized each cable using multiple truss elements. Such modeling is appropriate in the case of small bending stiffness and small sag at equilibrium. The Green Lagrange formulation is used to reproduce large deformations, and the axial strain is computed by expressing the global strains in tangential derivatives and projecting the global strains on the cable edge. Paolo Lonetti and Arturo Pascuzzo investigated in another study the description of the formulation to predict optimum post-tensioning forces and cable dimensioning for self-anchored cable-stayed suspension bridges [24, 25]. They also adopted and explained (MECS) approach. Raid Karoumi presented in his study a method for modeling cable-stayed bridges for nonlinear finite element analysis (FEA) [19]. Catenary cable element is an approach that is adopted to consider the change of cable geometry under different tension load levels (cable sag effect) in which exact analytical expressions for the elastic catenary is used. This approach was also used in [20]. Complexity is faced as cable-stayed bridges are analyzed as three-dimensional structures [3]. However, some studies made simplified assumptions on boundaries on the bridge deck to minimize the issue to a two-dimensional study [31].

Wilson and Gravelle presented approaches for modeling cable-stayed bridges in a linear finite element model for dynamic analysis. In their study findings, a linear model can work well for modeling and analyzing [36]. Wilson and Liu said that a linear elastic finite element model is able to capture with great precision much of the complex dynamic behavior of the cable-stayed bridge, compared to low complex reactions caused by environmental wind and excitations in traffic [37].

Few studies have been conducted to investigate the effect of pylon shape variation. Almas and Rajesh [2] performed 3-D models using straight and curved bridge cable-stays with A-shape, H-shape, and inverted Y-shape pylons. Modeling was performed using ANSYS software. It was concluded that the inverted Y-shaped pylon is naturally more appropriate for both curved and straight cable-stayed bridges. Shah et al. [30] performed linear and nonlinear analyses for bridges supported by three different configurations such as H-shape, A-shape & inverted Y-shape under aerostatic loading. They concluded that the H-shape gives higher straining action than the inverted Y-shape and the A-shape. That makes the conventional H-shape to be the most demanding shape. Thakkar [33] performed dynamic and aerostatic analyses on different shapes of cables-stayed pylons. This analysis was formed for different main span lengths (200, 400, 600, 800 m). He found that the increase in span increases the axial tensile force in the cable. This is because the segment length and the depth increase, so the weight of the deck increases and thus the axial force in the cables. The delta shape of the pylon has less forces than others in both the Linear and Dynamic cases

for Girder axial force, while in terms of shear and pylon torsion, both H shape and A shape shaped pylons perform better, and in terms of pylon moment, the Inverted Y shape, as well as H-shape and A-shape, perform better.

The current concept in the analysis and designing of cable-stayed bridges considers freeing decks from the lower strut of pylons, especially in areas of frequent earthquakes. It was observed that induced forces at the lower strut level are very high in the transverse direction [5, 6]. During the Chi-Chi earthquake (Taiwan1999), it was obvious that the reason behind damage to the tower of Chi-Lu Bridge was a transverse induced force. It was considered that the largest damage ever reported resulted from the earthquake [8]. Unfortunately, studies that concentrate on cable-stayed bridges' transverse seismic response are few. Camara and Efthymiou [7] performed dynamic analysis to investigate the force induced due to seismic loading in a transverse direction in the deck tower connection, as the common design to make deck tower connection in transverse direction fixed. Though the technique of base isolation has been successfully implemented worldwide for buildings and short to medium-span highway bridges only a limited amount of work has been conducted on the base isolation systems used for the seismic control of cable-stayed bridges [4, 22]. Ali and Abdel-Ghaffar [1] investigated the effectiveness of elastomeric bearings (both elastic and hysteretic types) for seismic isolation of cable-stayed bridges. They observed that a significant reduction in the seismic forces induced on bridges can be achieved through the installation of the hysteretic energy dissipation devices at appropriate locations. Wesolowsky and Wilson [35] examined the efficacy of using seismic isolation with LRB to favorably influence the seismic response of cable-stayed bridges subjected to near-field earthquake ground. Soneji and Jangid [32] investigate the effectiveness of elastomeric and sliding types of isolation systems for the seismic response control of cable-stayed bridges. A simplified two- dimensional lumped-mass finite-element model of the Quincy Bay-view Bridge at Illinois was developed for the investigation. The seismic isolation of cable-stayed bridges is achieved using three different isolators, namely, high damping rubber bearings (HDRB), lead rubber bearings (LRB), and friction pendulum system (FPS).

There are no guidelines in the design codes related to pylon shape or deck width for cable-stayed bridges. The E.C.P 207 [11, 12] gave some guidelines:

- The effective stiffness of elements is the same as the gross stiffness with no reduction (no cracks allowed).
- It is recommended that the main spans from 100 to 200m have a force induced in the cable from adding live load $\leq$ 30% of the cable's design force and the force in cables is $\leq$ 45% of the cable breaking force.
- It is also recommended for the assumption of side span length and assumption of pylon height above the deck to be as shown in Fig. 1.

Eurocode [9, 10] also give a few recommendations.

- For cable-stayed bridges dominated by high modes, the behavior factor should be equal to1

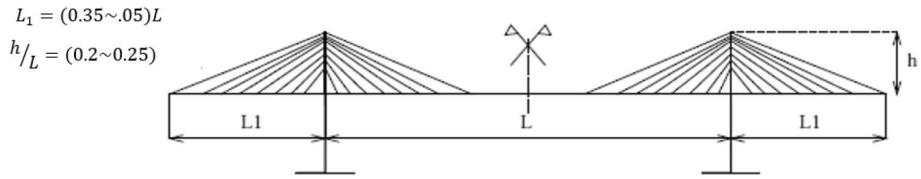

Fig. 1 E.C.P recommendation for side span length and pylon height (E.C.P part5 2015)

- Performing of the plastic hinge should be avoided in that type of bridges
- The force in cable $\leq$ 45% of the breaking force of cable

AASHTO LRFD and ACI codes didn't give any recommendations on pylon shape or deck width.

The key purpose of this study is to make proposals for the design of cable-stayed bridges due to seismic loads. 3-D finite element models were performed using numerical analysis to study the behavior of different pylon shapes under static and seismic loads. Also, this study presents a methodology to follow when designing cable-stayed bridges to estimate the deck width for a certain main span length.

Methods (parametric study modeling and assumptions)

The objective of this work is to investigate the pylon shape performance under seismic loads as well as the deck width effect on induced transverse shear force from seismic loading. The analysis is performed using Midas-Civil software. The assumptions considered in the analysis are as follows:

- It is assumed that the joint between the cable, girder, and tower is a pinned joint.
- It is assumed that the sagging effect is ignored for the case under investigation. Previous research efforts suggested the same assumption [21]. The equation of Ernst of modifying the modulus of elasticity in the equation [34] can be used. The equation can consider the sag effect.
- It is assumed that the structure remains linearly elastic.
- It is assumed that the conditions used to get preliminary forces in the cable before starting any analysis are displacement for nodes of cross-girders of the deck ($\pm$ 1 cm) in vertical direction and displacement of pylon top node ($\pm$ 5cm). The deformed shape of the deck is then compared across all models to ensure that it is the same, in order to keep that parameter constant under initial conditions.
- It is assumed that in all the parametric study models, the transverse deformation of the deck is ignored as the deck is represented as a spin mode (the deck section is defined as one frame element).
- It is assumed that the cross-girder is defined only as a nodal load, ignoring its stiffness, which affects transverse deformation and simplifies the comparison.
- It is assumed that for different main span lengths, the main girder dimensions should be slightly changed as the influence of the live load isn't as uniform as the influence of the dead load. In this analysis, it is assumed to be the same to enable the comparison.

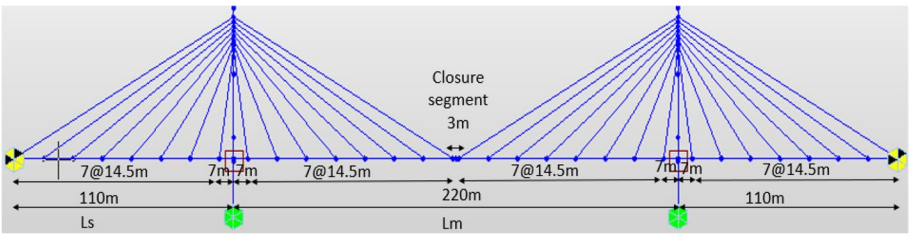

Fig. 2 Layout for the 1st parameter cable-stayed bridge

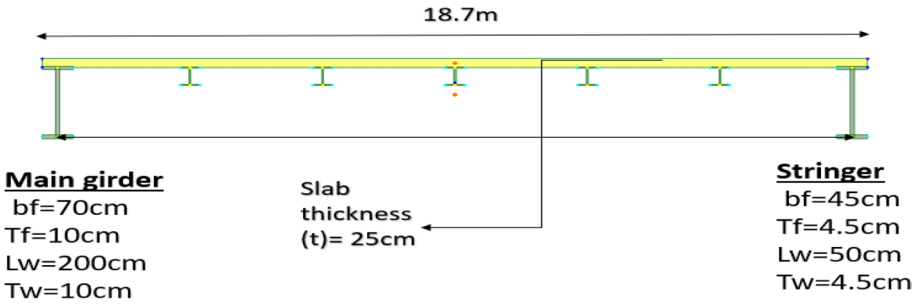

Fig. 3 Typical section of concrete deck

- It is assumed that the straining actions of each of the two legs of pylon shapes with four legs are added to each other to be compared to pylon shapes with two legs.

Bridge layout

The bridge used in this study is a floating cable-stayed bridge (which means that both the main span and side span are composite steel girders with concrete deck). The bridge dimensions are shown in Fig. 2.

Bridge deck

The deck consists of a composite steel-concrete system as shown in Fig. 3. It consists of outer main girders and stringers between them. These main girders are connected together with stringers in the transverse direction by cross girders. The precast reinforced concrete deck is made up of all of these girders.

Modeling of the bridge

This study shows most of the shapes of the pylon that are adopted in the construction and design of new cable-stayed and most of the existing cable-stayed bridges. The performance of the eight pylon shapes (A-shape, A-D shape, inverted Y-shape, inverted Y-D shape, delta shape, pyramid shape, H-shape, and inclined H-shape) will be compared. Pylons have some different dimensions since each shape has its own configuration for cable. The distance between cables in a pylon is constant, but the pylon legs will converge or diverge depending on the shape as shown in Fig. 4. The deck width is

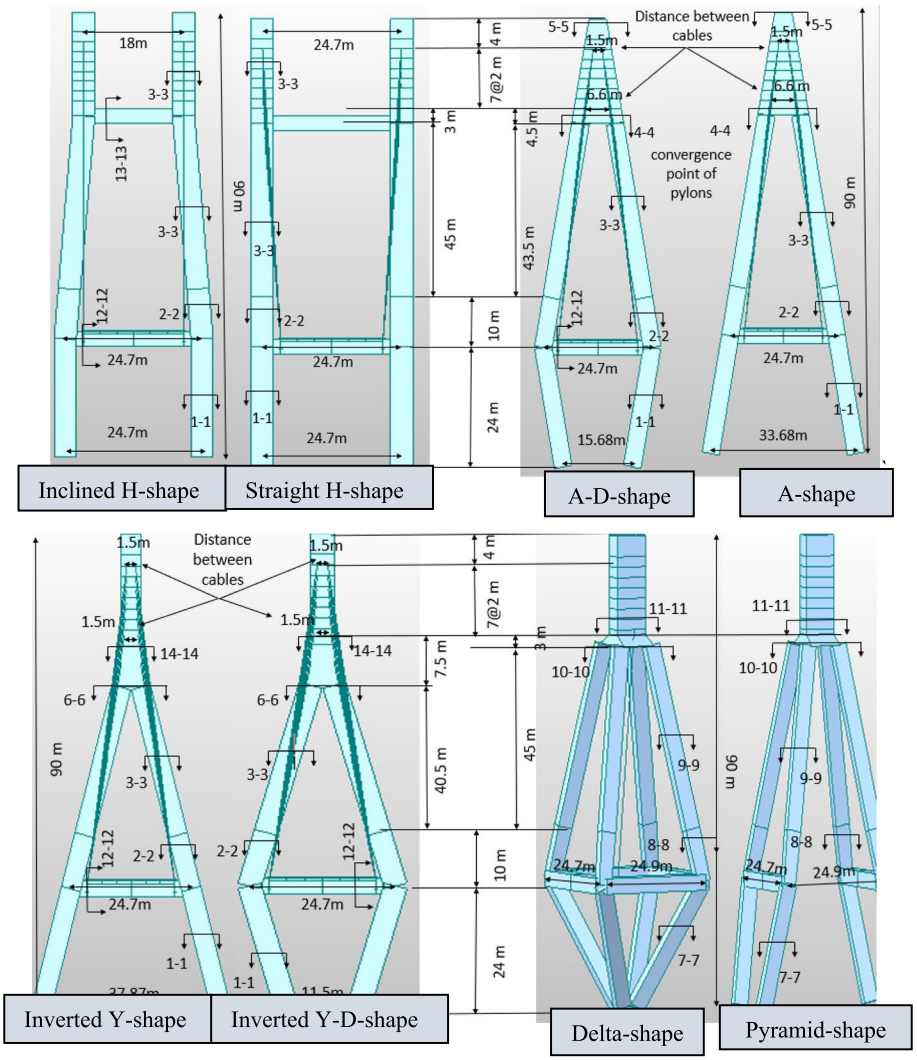

Fig. 4 Detailed pylon shapes and dimensions used in 1st parametric study. Note: all dimensions are measured from center line to center line for any element

equal to 18.7 m and there is a 1 m free distance between the deck and the edge of the pylon deck. The width of the pylon leg is 4 m. The first cable is located at 4 m from the top of the pylon followed by, equally located cables. The distance between them is 2 m and the total height of the pylon is 90 m. The ratio between H_p/L_m is constant equals 0.3 and the ratio between L_s/L_m is constant equals 0.5. Where Hp refers to the height of the pylon above deck. Lm refers to main span length and Ls refers to side span length. Section 1-1 intersects the center line of the lower tie beam at a distance of 24 m from the base. Then there is 10 m variable section (2-2). For H shapes, the pylon continues with the section that ended by section (3-3). Upper strut beam is located at level 69 m from the base for H-shape. A-D shape point of intersection of converged pylons is at 69 m from the base for A. For Y, Y-D, delta, and pyramid shapes, the point

Table 1 Detailed pylon cross-section dimensions

Sec - No.	Type	Dimension (m)					
	1	A			B		
1-1		7m			4m		
7-7		3.5m			2m		
12-12		5m			3m		
	2	A		B	C		D
2-2		7m		4m	0.5m		0.5m
3-3		7m		4m	2m		5m
8-8		3.5m		2m	0.25m		0.25m
9-9		3.5m		2m	1m		2m
10-10		14.4m		11.6m	9.8m		12.6m
11-11		7.5m		5.5m	3.7m		5.7m
13-13		5m		3m	1m		3m
	3	A	B	C	D	E	F
4-4		11.86m	7m	2m	5.86m	1m	1m
5-5		4m	7m	0.9m	0.2m	1m	1m
6-6		8m	7m	2m	2m	1m	1m
14-14		4m	7m	0.9m	0.2m	1m	1m

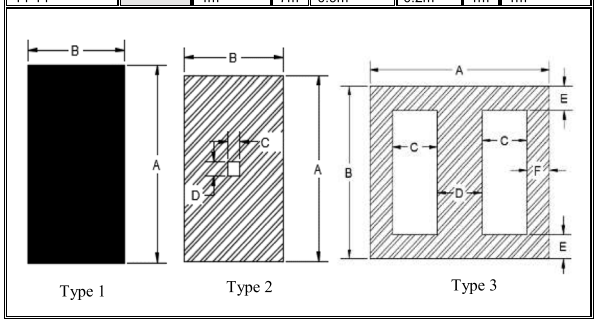

of intersection is located at 61.5 m from the base. Y, Y-D, delta, and pyramid shapes also have tapered sections after intersection for 7.5 m to reach the same level as other shapes (69 m from the base). Cross-sections are shown in Table 1.

Cable layout for the bridge is as shown in Fig. 2. Figure 5 shows the cable labels where the cross-sectional area for each cable: Cable 1= 0.0055 m^2, Cable 2= 0.00667 m^2, Cable 3= 0.00754 m^2, and Cable 4= 0.00859 m^2.

There are two bearings under deck with different allowed movements and the same for end bearings at abutment as shown in Fig. 6. While the pylon base is fixed in six degrees of freedom (D.O.F). Properties of material used in those models are shown in Table 2.

Effect of deck width

The analysis sequence considering this parameter sequence is conducted as shown in Fig. 7. For each main span length, there are four models with different deck width. The reason for choosing those main span lengths is that span length is duplication of distance between cables. For deck width, two stringers with the same spacing are added for each deck width. The inverted Y-shaped is the shape on which this study was performed. The ratio between $H_p/L_m$is taken as constant equals 0.3, and the ratio between $L_s/L_m$is constant equals 0.5.

Pylon

The inverted Y-shape is adopted in this study. To keep the ratio mentioned above, the constant pylon height is changed as shown in Fig. 8. The dimensions of the pylon

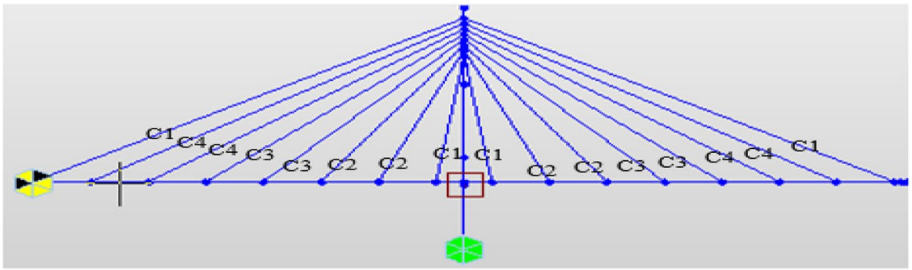

Fig. 5 Stay cables label and arrangement

and the number of cables in the model (side span and main span) are shown in Fig. 8. Cross-section of the pylon for the inverted Y-shape is detailed in Table 1.

Bridge deck modeling

Deck was modeled as a spin model as mentioned in Hambly's book [14] for composite sections. The cross-girder is represented as nodal load. The cross girder is used to connect the two cable anchor points on the deck. This nodal load force is equal to a number resulting from multiplying 7.4 kN/m by deck width. This uniform load represents the own weight of steel cross-girder per meter. The dimensions of deck slab thickness, stringers, and main girder are the same. The spacing of cables and spacing between stringers are the same.

Cables

Figures 9, 10, 11, and 12 show the number of cables. The number of cables related to its cross-sectional area. The different cross-section areas result from the form finding

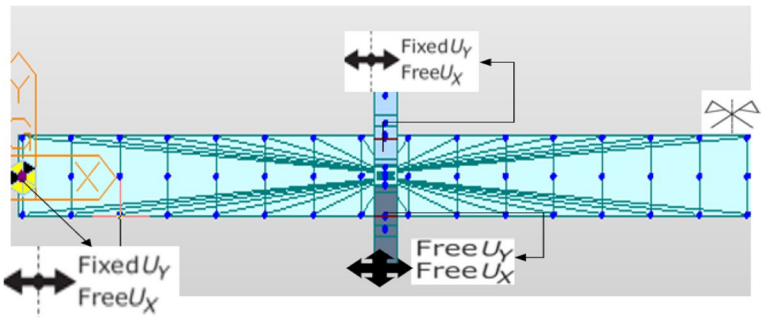

Fig. 6 Bearing's allowable movements direction (plan view)

Table 2 Material properties

S.N	Member	Material	Weight (kN/m^3)	Poisson ratio	Modulus of elasticity (GPa)	Stress (MPa)
1	Pylon	RC	25	0.25	35	65 (compressive)
2	Slab	RC	25	0.25	25	35 (compressive)
3	Girder	steel	77.09	0.3	199	250/450 (yield/ultimate)
4	Cable	steel	77.09	0.3	198	1860 (ultimate)

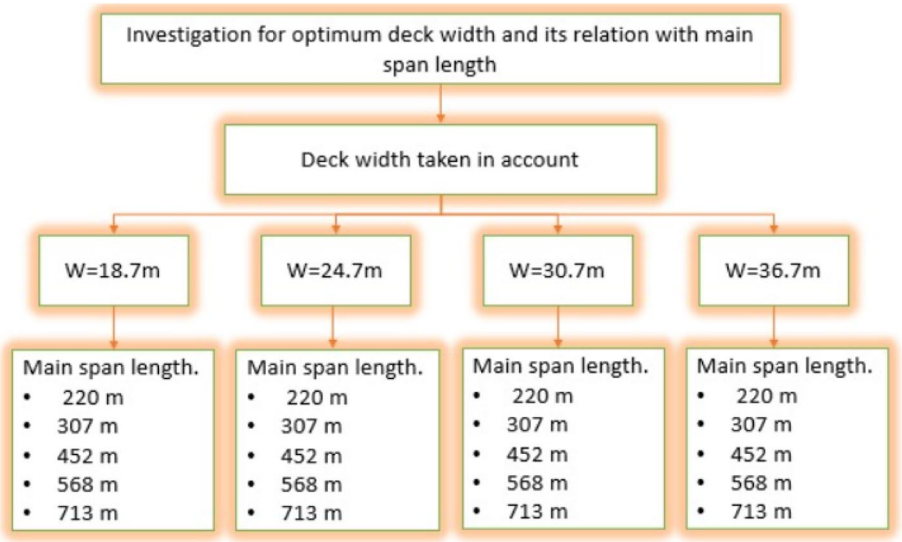

Fig. 7 Detailed scope for the 2nd parameter (deck width effect)

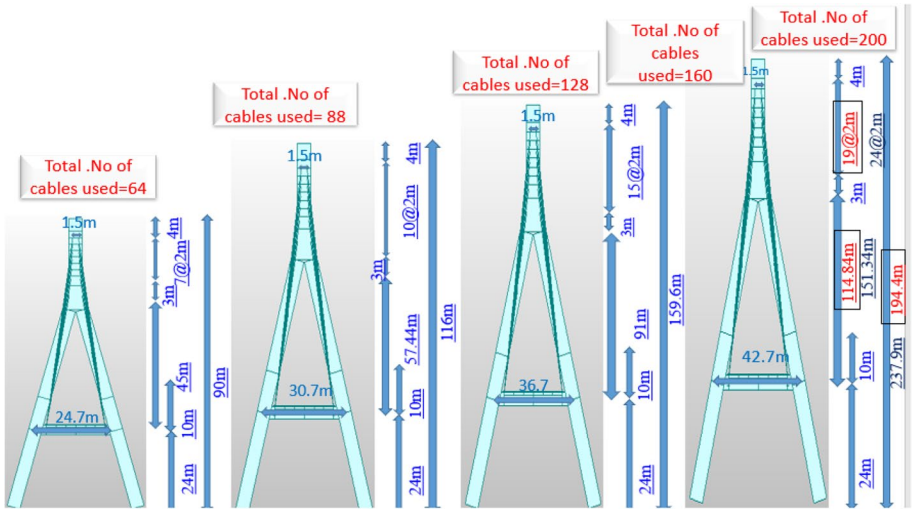

Fig. 8 Dimension of pylons for different models

step (refer to the "Form finding" section). The stress in the cable is kept within the code-recommended range.

Loads

The static loads are taken the same in the two parametric studies. These are: self-weight, barrier load = 5 kN/m/side & SIDL (asphalt thickness = 100 mm).

The dynamic load considered in the first parametric is the response spectrum of the ECP (207) code [11, 12] in which response type (2), soil type (A), zone (3), peak ground acceleration ag = 0.15g, impact factor =1, and a reduction factor of R=1. In the

second parametric study, the dynamic load is modal response spectrum analysis (MRSA) according to Eurocode [9, 10]. This analysis was performed on each model in which the response type (1), type soil (A), peak ground acceleration ag =0.5g, impact factor =1, and reduction factor taken R=1.

Form finding

In the design of long span structures, the problem is often faced where a solution to unknown loading conditions is necessary to satisfy a given design requirements. Midas Civil program is capable of solving this type of problem using an optimization technique by calculating the optimum variables for given constraints and object functions. For constraint conditions, equality and inequality conditions are permitted.

The form finding stage is the first stage of any analysis. In this study, the form finding stage was performed based on inequality conditions. These conditions are to allow maximum vertical movement of deck ± 10mm and displacement of the top of the pylon in the longitudinal direction of the bridge ± 50mm.

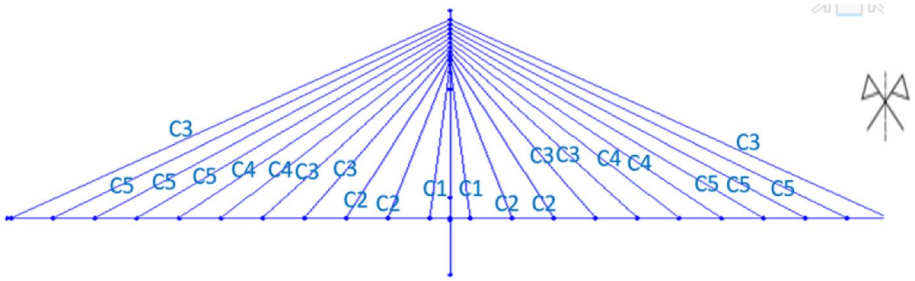

Fig. 9 Stay cables label, arrangement & cross-section for main span 307 m. Where Cable 1= 0.0046 m^2, Cable 2= 0.0065 m^2, Cable 3= 0.008 m^2, Cable 4= 0.009 m^2, and Cable 5= 0.01 m^2

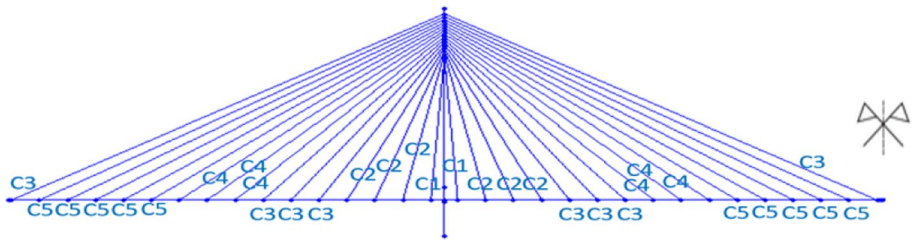

Fig. 10 Stay cables label, arrangement and cross-section for main span 452m. Where Cable 1= 0.0045 m^2, Cable 2= 0.0063 m^2, Cable 3= 0.0072 m^2, Cable 4= 0.0085 m^2, and Cable 5= 0.01 m^2

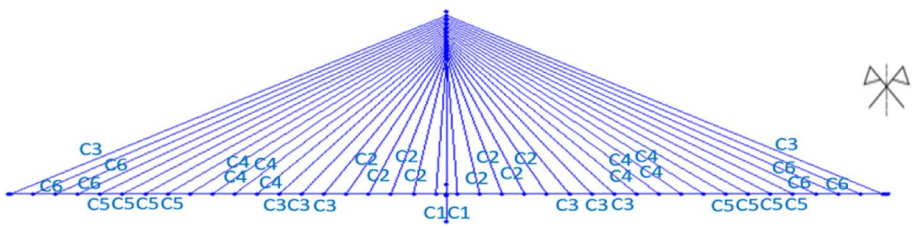

Fig. 11 Stay cables label, arrangement & cross-section for main span 568m. Where Cable 1= 0.0045 m^2, Cable 2= 0.0063 m^2, Cable 3= 0.0072 m^2, Cable 4= 0.0082 m^2, Cable 5= 0.01 m^2, and Cable 6= 0.011 m^2

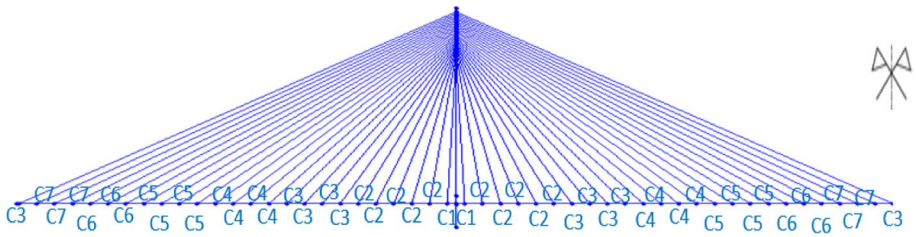

Fig. 12 Stay cables label, arrangement & cross-section for main span 713m. Where Cable 1= 0.0045 m^2, Cable 2= 0.0063 m^2, Cable 3= 0.0072 m^2, Cable 4= 0.0082 m^2, Cable 5= 0.009 m^2, Cable 6= 0.01 m^2, and Cable 7= 0.011 m^2

These conditions are under uniform load, which represents dead load. Figure 13 shows the deck profile for two pylon shapes' models of the pylon effect study. The maximum difference in deformation of any point in the deck is± 5mm. Figure 14 shows the top pylon deformation for the form finding. Figure 15 shows the labels of cables which will be used in other figures. Figure 16 shows the force in the cables of the form finding.

For cable forces, there are some forces for Y, Y-D, and pyr/diam which are high to maintain the same constraints applied for all models, but it is reflected by lower force in cables before and after that cable.

Validation

Validation is performed on the Quince Bridge, which crosses the Mississippi river in Illinois, USA. This bridge was selected since its geometry and all the needed information are well documented by Wilson and Gravelle [36] and Wilson and Liu [37]. It was also used as validation in some studies in Hariri [15], Niyitegeka [26], Sarhang Zadeh [29], Hua and Wang [17], and Poddar and Rahman [27].

To validate the finite element of the Quincy bridge in this study, the dynamic characteristics of the bridge from the Midas civil model were compared to those provided by Hariri [15], Hariri and Lin [16], Niyitegeka [26], Wilson and Gravelle [36], Wilson and Liu [37]. In 1991, two papers were published on Quincy cable-stayed bridge by Wilson. In the first paper, Wilson and Gravelle [36] conducted finite element model and obtained the mode shapes and frequencies. In the second paper, Wilson and Liu [37] installed microsensors to monitor the response of the bridge due to vibrations. They also examined the bridge's dynamic response. In 2016, Niyitegeka [26] studied the effect of pylon shapes on the static and dynamic response of cable-stayed using the Sap2000 program. In 2018, Hariri [15] and Hariri and Lin [16] studied the resonance of cable-stayed bridges subjected to delayed time-histories using multi-support excitation using the Sap2000 program. Mode shapes and modal frequency are compared for the above-mentioned work for validation in Table 3 and Fig. 17a, b.

Mode shapes

Figure 17a, b depict the mode shapes of the Quincy bridge. Such shapes provide good coloration to that referenced in Wilson and Gravelle [36], Wilson and Liu [37], and Hua and Wang [17]. FEM was used in [13] to get mode shapes. Wilson and Liu [37] made

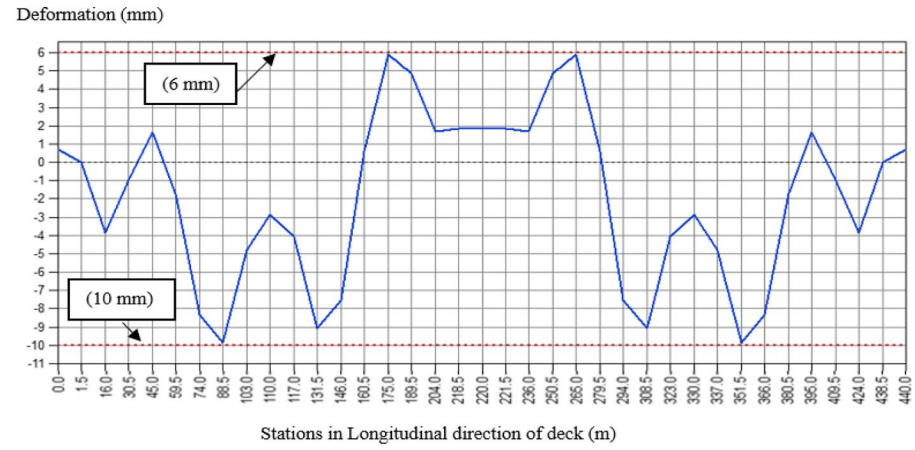

a-Displacement of Deck of A-shape Pylon Bridge Model

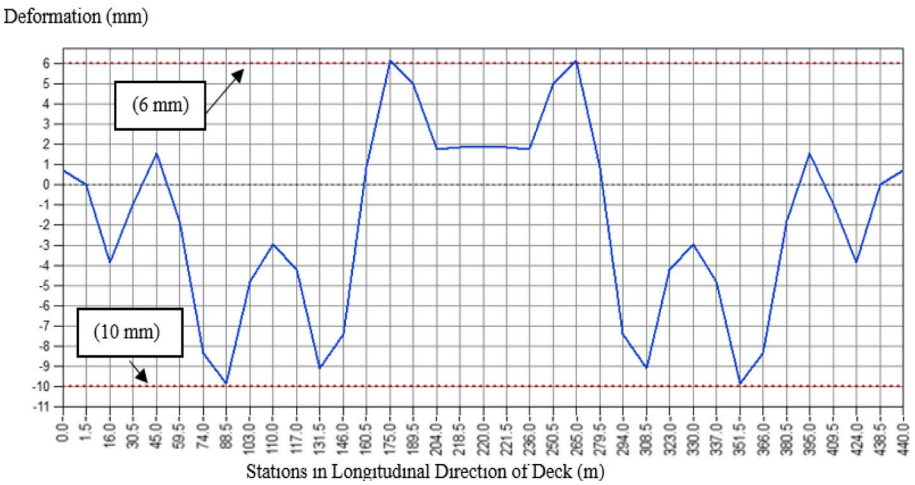

b-Displacement of Deck of A-D-shape Pylon Bridge Model

Fig. 13 Deck movement after getting the cable forces by unknown load factor. **a** Displacement of deck of A-shape pylon bridge model. **b** Displacement of deck of A-D-shape pylon bridge model

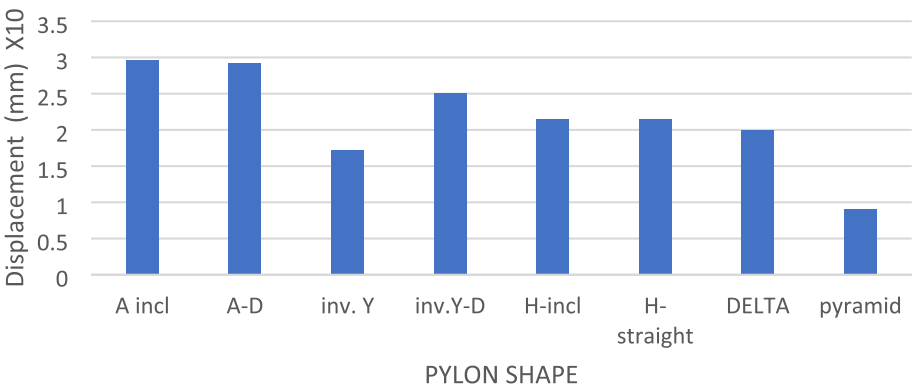

Fig. 14 Displacement of pylon towards main span resulted from form finding

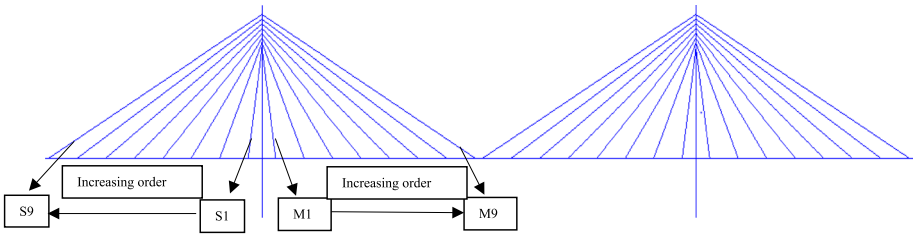

Fig. 15 Cable labels

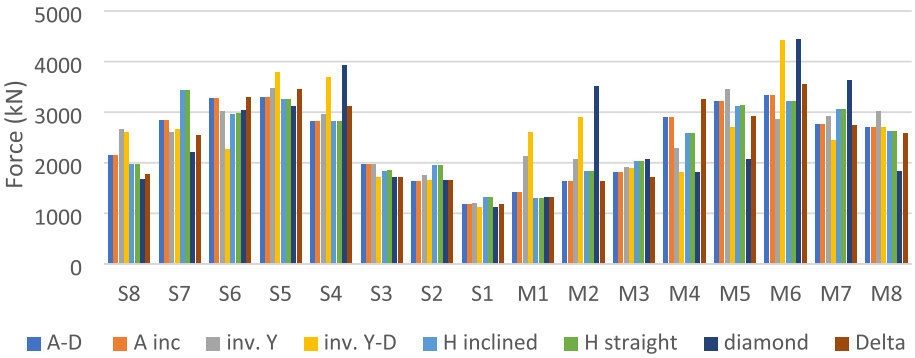

Fig. 16 Force in cables of each pylon shape model from form finding

tests on the Quincy bridge to get mode shapes. In Hua and Wang [17], numerical model on sap2000 was created to get mode shapes.

Results and discussion

The SAG effect was taken into account according to the Ernst equation, and the results were compared to those of the case of neglecting its effect. This comparison shows the changes in the frequency for each mode. The comparison is shown in Table 4 for cable-stayed bridges of A-pylon and A-D pylon shapes. The change in frequencies is very small and does not affect the bridge behavior. Hence, in this investigation, the sag effect can be neglected.

Pylon shape effect results

Performance of bridges of different pylon shapes (forces in cables due to different directions of response spectrum, and straining action on pylons' legs) was obtained.

Figure 18 shows the comparison of effect of MRSA in a longitudinal direction. The results show that the pyramid shape gives a higher response in most cable forces due to the response spectrum in the longitudinal direction followed by the inverted Y-shape nd then followed by the inverted Y-D shape. The rest of the shapes are nearly the same as shown in Fig. 18.

Figure 19 shows comparison of effect of MRSA in transverse direction. The result shows that the inverted Y-shaped shape gives a higher response in most of the cable forces due to response spectrum in transverse direction followed by pyramid shape and then the delta shape. The rest of the shapes are nearly the same as shown in Fig. 19.

Table 3 Comparison between frequencies from different studies of Quincy bridge

Mode Shape	Wilson 1991 [36, 37]		Hariri [15] SAP 2000	Niyitegeka Simon [26]	Current study Midas 2019
	Freq. (cyc/sec)		Freq. (cyc/sec)	Freq. (cyc/sec)	Freq. (cyc/sec)
	Fin. elem	TEST			
1	0.371	0.375	0.374	0.368	0.377
2	0.500	0.500	0.498	N/A	0.481
3	0.577	0.560	0.587	0.571	0.570
4	N/A	0.630	0.654	Only compared for those two modes only	N/A
5	0.633	0.740	0.760		0.760
6	N/A	0.740	N/A		N/A
7	0.770	0.800	0.833		0.754
8	N/A	0.809	N/A		N/A
9	0.864	0.890	0.973		0.850
10	0.733	0.890	0.966		0.868
11	1.023	1.055	1.122		1.000
12	0.949	1.110	1.041		1.081
13	1.023	1.180	1.158		1.212
14	1.297	1.375	1.327		1.239
15	1.150	1.400	1.305		1.252
16	1.345	1.430	1.403		1.313
17	N/A	1.440	1.333		1.329
18	1.383	1.460	1.452		1.337

Figure 20 shows a comparison of the effect of MRSA in a vertical direction. The results show that all shapes approximately give the same response in cable force due to the response spectrum in a vertical direction as shown in Fig. 20.

Pylon straining action for combination (C1)

The main seismic longitudinal direction results (longitudinal moment and shear force, and torsional moment as a result of this combination.

Figure 21 shows the longitudinal moment at the base of C1. The results show that A and A-D shapes give a high response compared to other shapes for a moment around the transverse direction. Pyramid and delta shapes give the lowest moment around the transverse direction as shown in Fig. 21.

Figure 22 shows a longitudinal shear force at the base of C1. The results show that A-D, inclined A, straight-H, and inclined H shapes give nearly the same result. Pyramid shapes give the best performance followed by delta shapes as shown in Fig. 22.

Figure 23 shows the torsional moment at the base of C1. The results show that inverted D and A-D suffer from the highest torsion approximately double the response of other pylon shapes. Pyramid, straight H, and delta shapes give the lowest torsion A, and A-D shapes give high response compared to other shapes for a moment around the transverse direction. Pyramid and delta shapes give the lowest moment the around transverse direction as shown in Fig. 23.

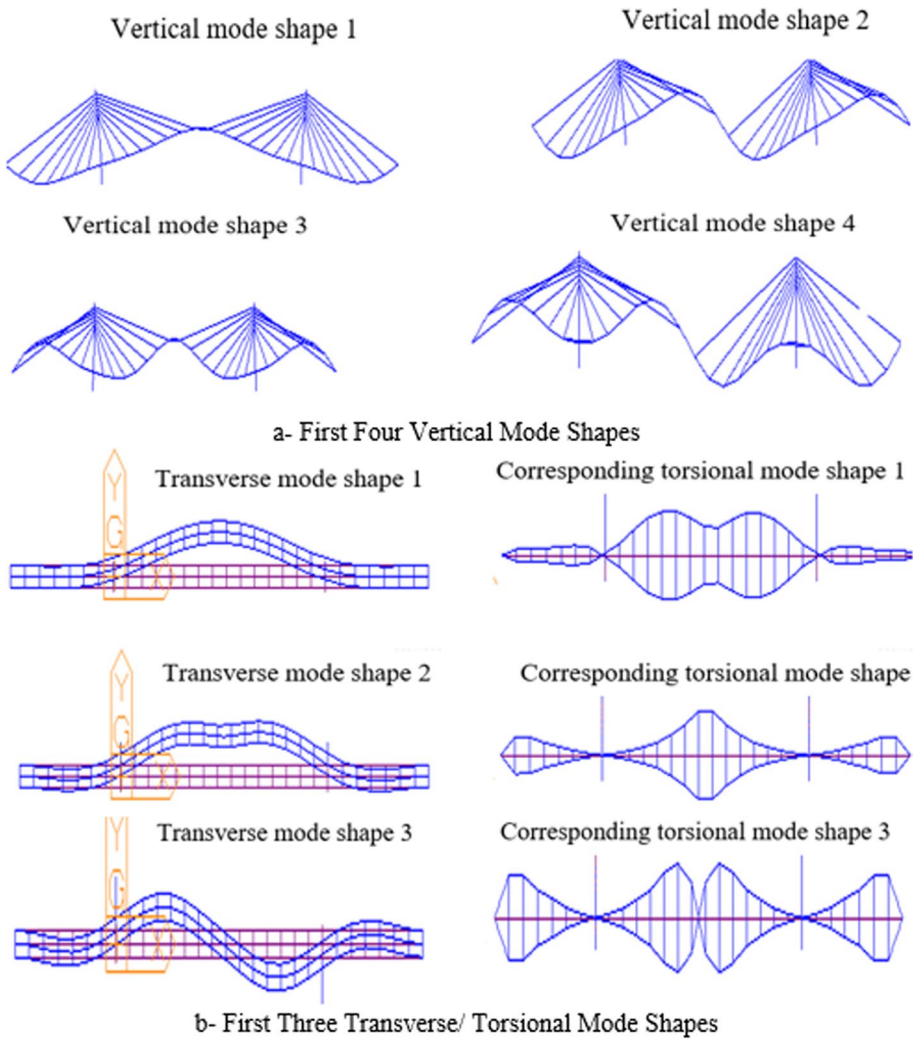

Fig. 17 Mode shapes. **a** First four vertical mode shape, **b** First three transverse/torsional mode shapes

Table 4 Comparison of mode shape frequencies for A- and A-D-shape pylon with and without sag effect

A-inclined			Difference (cycle/sec)	A-D inclined			Difference (cycle/sec)
Mode No.	Ignoring sag effect	Taking sag effect		Mode No.	Ignoring sag effect	Taking sag effect	
	Frequency (cycle/sec)				Frequency (cycle/sec)		
1	0.452715	0.448629	0.003914	1	0.45156	0.447624	0.003936
2	0.506174	0.506163	0.000011	2	0.505474	0.505459	0.000015
3	0.635336	0.635246	0.0029	3	0.634883	0.63197	0.002913
4	0.995691	0.992758	0.002933	4	0.796518	0.797282	0.000764
5	1.09261	1.09112	0.001482	5	0.896326	0.897728	0.001402

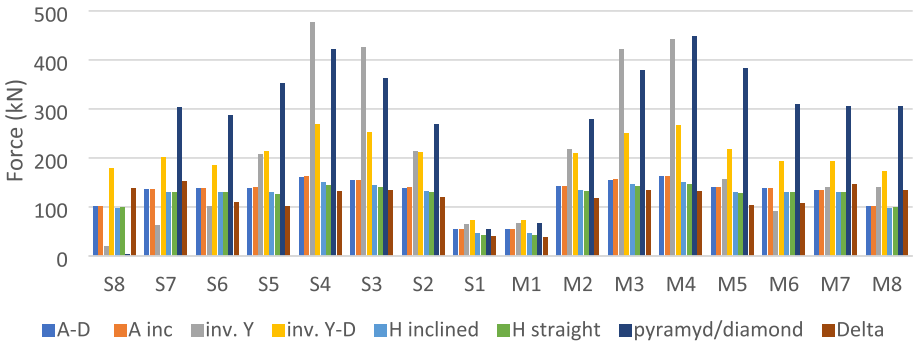

Fig. 18 Comparison of effect of MRSA in longitudinal direction only on cable forces due RSX

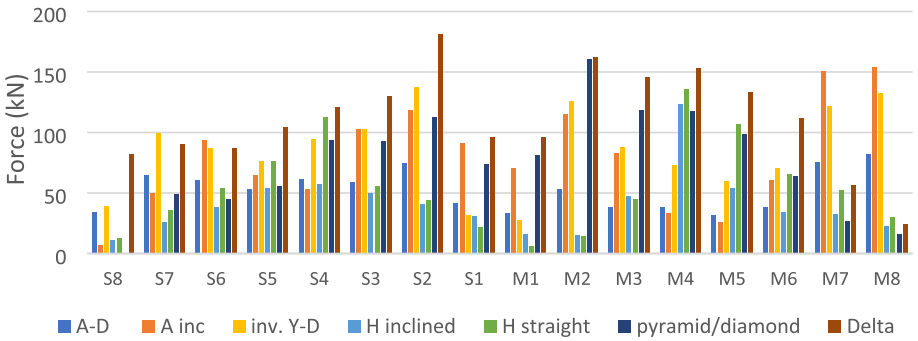

Fig. 19 Comparison of effect of MRSA in transverse direction only on cable forces due RSY

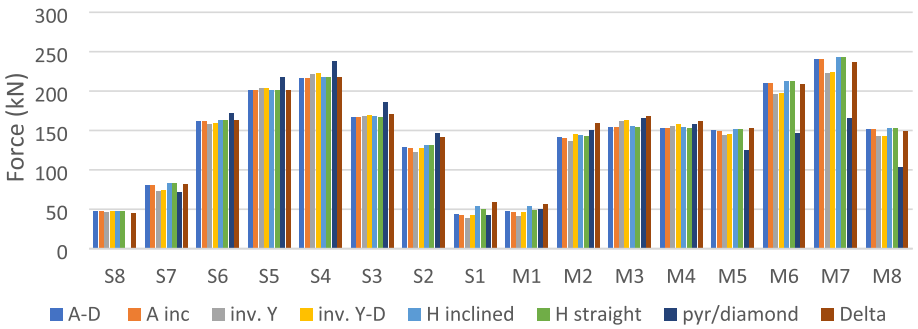

Fig. 20 Comparison of effect of MRSA in vertical direction only on cable forces due RSZ

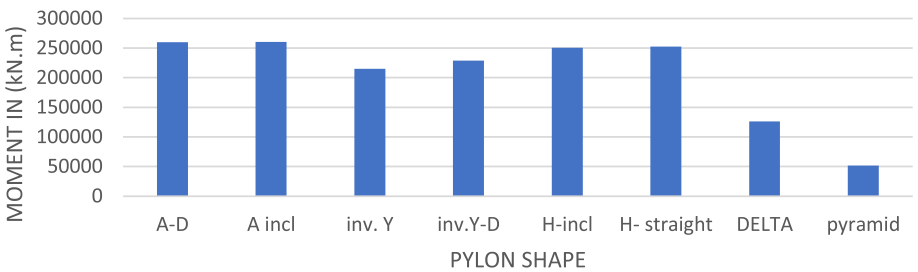

Fig. 21 Longitudinal moment at base of C1

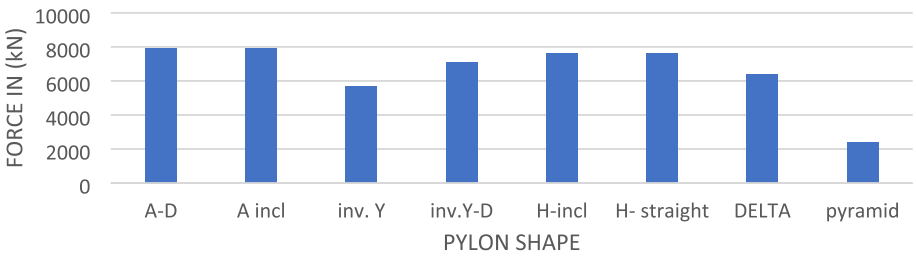

Fig. 22 Longitudinal shear force at base of C1

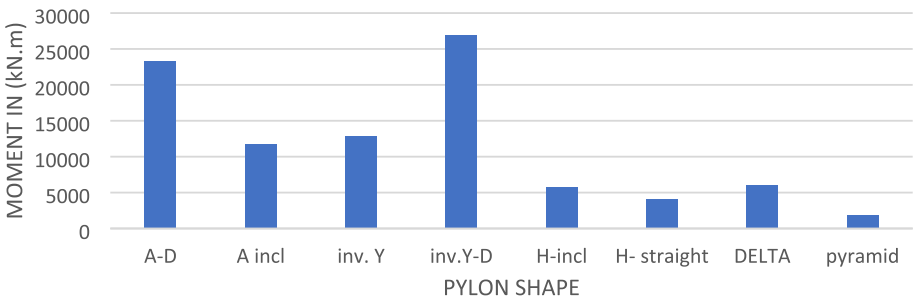

Fig. 23 Torsional moment at base of C1

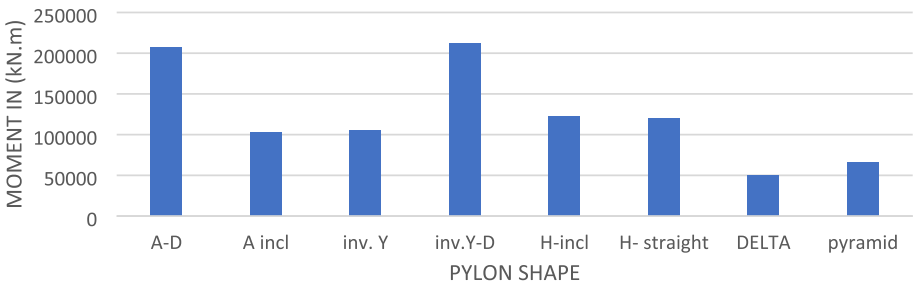

Fig. 24 Transverse moment at base of C2

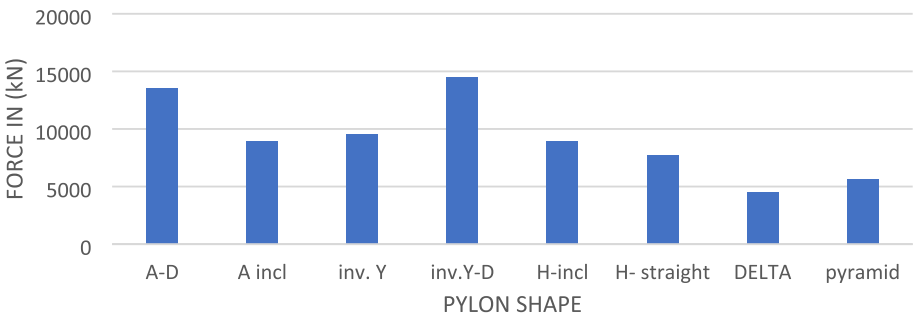

Fig. 25 Transverse shear force at base of C2

Pylon straining action of combination (C2)

The main seismic transverse direction results transverse moment and shear force and torsional moment as a result of this combination.

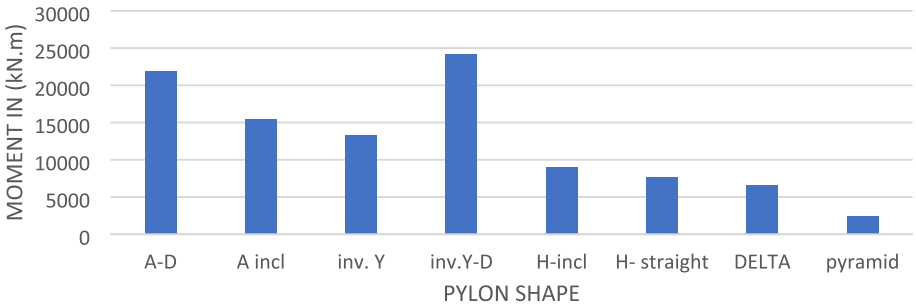

Fig. 26 Torsional moment at base of C2

Figure 24 shows the transverse moment at the base of C2. The results show that inverted Y-D and A-D shapes give a high response compared to the other shapes for a moment around the longitudinal direction. Delta and pyramid shapes give the lowest moment around longitudinal direction as shown in Fig. 24.

Figure 25 shows a transverse shear force at the base of C2. The results show that inverted Y-D and A-D suffer from the highest transverse shear followed by inverted Y and inclined A shapes. Pyramid and delta shapes give the lowest transverse shear as shown in Fig. 25.

Figure 26 shows the torsional moment at the base of C2. The results show that inverted Y-D and A-D suffer from the highest torsion followed by inverted Y and inclined A shapes. Pyramid and delta shapes give the lowest torsion as shown in Fig. 26.

Effect of deck width variation

The analysis shows that there are certain modes that dominate in the transverse direction. This finding is in good agreement with those of Camara and Efthymiou [7] as shown in Fig. 27.

This part of the study investigates shear force induced in the connection between deck and tower. Two types of soil were considered: soil type A according to Eurocode for the widths of 18.7m, 24.7m, and 36.7m as shown in Fig. 28a, b, and c.

The results show that the three dominating modes are shifted to the right (in the direction of increasing main span length) by increasing the deck width by tracing the arrow in Fig. 29.

Shear force in the transverse direction is calculated by Complete Quadratic Combination (CQC) method as shown in Fig. 30. The results show that the shear force decreases at main span length = 452m for all deck widths used except for deck width = 36.7 m. Bridge with a main span length equal to 568m has the least shear force. The shear force increases by increasing the deck width as the participating masses increase.

To fairly compare results, the shear force is normalized since the masses are changed in various models as the deck width increased and the ratio between height and the main span is kept constant as shown in Fig. 30.

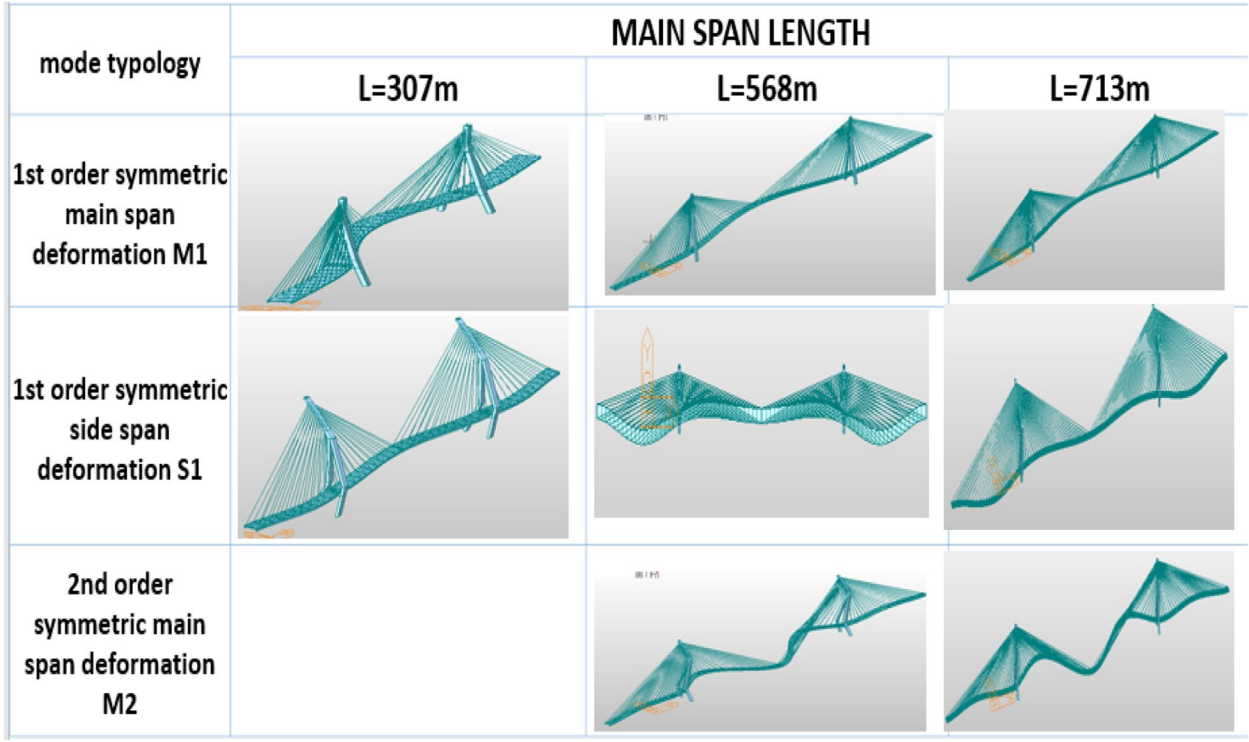

Fig. 27 Mode shape dominating in transverse direction

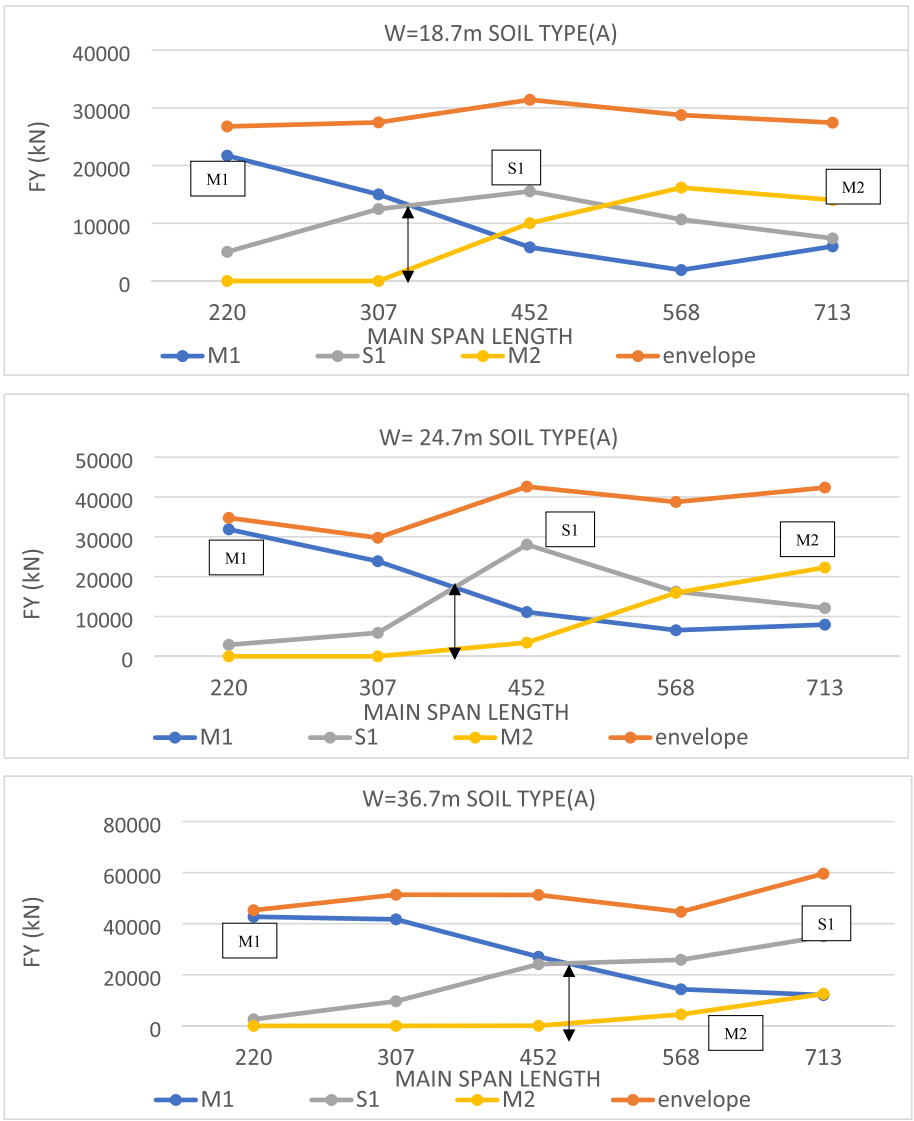

Fig. 28 Shear force induced from dominating mode shapes in the transverse direction with a variation of deck width with the main span

The normalized shear force decreases by increasing the main span length independent of deck width as each of the deck widths gives the same relationship [7].

$$W^Y = m_d\left(\frac{l_p + l_s}{2}\right)g$$

where

- m_d: represents the mass for unit length in deck which contributes.
- L_p: main span length, L_s: side span length.
- g = 9:81 m/s^2 is the gravitational acceleration

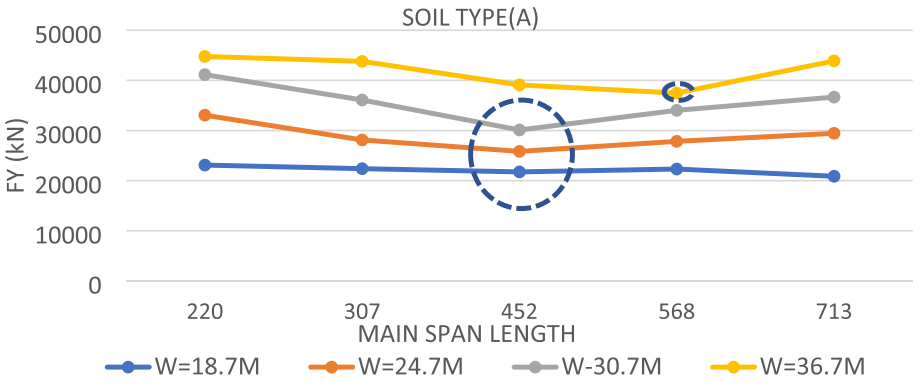

Fig. 29 Comparison between shear force induced from mode shapes in transverse direction for each deck width using CQC

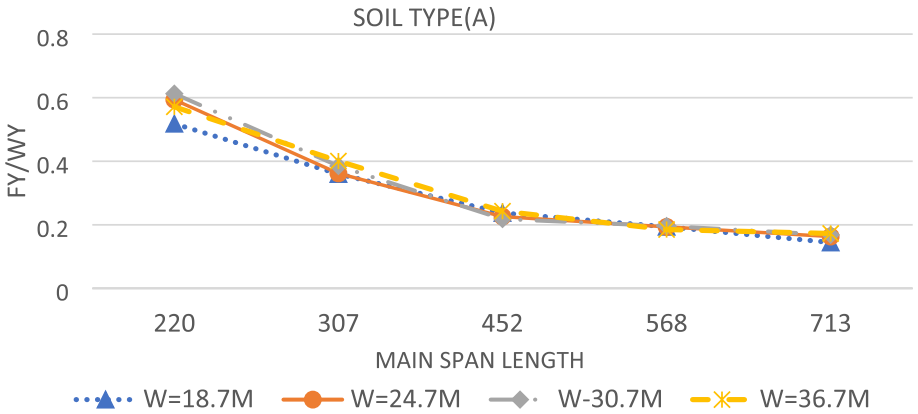

Fig. 30 Comparison between normalized shear force induced from mode shapes in transverse direction for each deck-width using CQC

Conclusions

This study focused on commonly constructed three-span cable-stayed bridges with a typical H_p/L_m ratio of 0.3. The ratio between L_s/L_m was considered to be a constant of 0.5. The cable-stayed bridge which has a floating deck was considered, but a non-floating (concrete) deck or semi-floating (hybrid) deck may have different responses.

The main conclusions derived based on the parametric study introduced are:

1. The sag effect can be neglected due to its small effect on frequencies leading to insignificant differences in results.
2. Pylons of Y-D & A-D shapes suffer from high values of the transverse moment, torsional moment, and transverse shear force. This is due to the decrease in stiffness that occurred in the pylon legs due to convergence, which resulted in the appearance of coupled-transverse modes in the early modes.
3. Under seismic loading in which the main direction is the longitudinal direction, the difference in straining action is as follows: the longitudinal shear force of pyramid shape is 29% to 40% of other shapes. The longitudinal moment of pyramid shape is

19% to 30% of other shapes; The torsional moment of pyramid shape is 8% to 28% of other shapes.

4. Under seismic loading in which the main direction is the transverse direction, the difference in straining action is as follows: the transverse shear force of pyramid shape is 38% to 73% of other shapes but larger than that of delta shape by 25%. The transverse moment of pyramid shape is 30% to 50% of other shapes but larger than that of delta shape by 30%. The torsional moment of pyramid shape is 10% to 37% of other shapes.
5. The recommendation categories of pylon shapes are as follows: pyramid shape is highly recommended, followed by delta, inverted Y, A, inclined H, and straight H shapes, respectively. Inverted Y-D and A-D shapes are not recommended from the seismic point of view.
6. There are three modes that dominate transverse response even if main span length or deck-width are changed: 1st order symmetric main span deformation (M1), 1st order symmetric side span deformation (S1), and 2nd order symmetric main span deformation (M2), respectively. As the deck width increases, the peak of these modes shifts to the right (increasing the main span length axis).
7. Transverse shear force induced at tie beam level from of deck widths (36.7, 30.7, 24.7) m to deck width (18.7m) are 190%, 170%, and 140%, respectively. This result is reasonable as the participating masses increase.
8. Normalized transverse shear force decreased by increasing the main span length. This force was independent on deck width as all deck widths give the same response. The transverse shear force could decrease by a more detailed investigation to determine two transitional zones between (M1 and S1) and (S1 and M2). This could decrease the transverse shear force to 72% to 82% of its initial value.

Abbreviations

MRSA	Modal response spectrum analysis
ECP	Egyptian Code of Practice for Planning, Design & Construction of Bridges
L_p	Main span length
AASHTO	American Association of State Highway and Transportation Officials
ACI	American Concrete Institute
H_p	Total height of the pylon
Ls	Side span length
R	Reduction factor
a_g	Peak ground acceleration
SIDL	Super imposed dead load
m_d	Represent the mass for unit length in deck which contributes.
W^y	Contributed weight in seismic loading.
kN	Kilo newton
M1	1st order symmetric main span deformation
S1	1st order symmetric side span deformation
M2	2nd order symmetric main span deformation

Acknowledgements

I would like to thank project manager Eng. Mohamed Fawzy for providing me with all of the information about the Rod El-Frag cable-stayed bridge.

In terms of the availability of data and materials, all data generated or analyzed during this study are included in this published article [and its supplementary information files].

Authors' contributions

"HA" and "KF" supervised the work in this manuscript & giving guild-lines to achieve the goal of this manuscript. The author(s) read and approved the final manuscript.

Funding
This research did not receive any specific grant from funding agencies in the public, commercial, or not-for-profit sectors.

Availability of data and materials
The datasets used and/or analyzed during the current study are available from the corresponding author on reasonable request.

Declarations

Competing interests
The authors declare that they have no competing interests.

Received: 10 March 2022 Accepted: 29 June 2022
Published online: 07 September 2022

References

1. Ali HEM, Abdel-Ghaffar AM (1994) Seismic energy dissipation for cable-stayed bridges using passive devices. Earthquake Eng Struct Dyn 23(8):877–893
2. Almas M, Rajesh A (2017) Effect of Pylon Shape on the Seismic Response of Curved and Straight Cable Stayed Bridges. Res J Adv Eng Sci 2(2):267–271
3. Baron F, Shen-Ying L (1973) Analytical studies of a cable stayed girder bridge. Comput Struct 3(3):443–465. https://doi.org/10.1016/0045-7949(73)90090-4
4. Buckle IG, Mayes RL (1990) Seismic isolation: history, application, and performance a world view. Earthq Spectra 6(2):161–201
5. Camara A, Astiz M (2011) Typological study of the elastic seismic behaviour of cable-stayed bridges. In: Paper presented at the Proceedings of the Eighth European Conference on Structural Dynamics
6. Camara A, Astiz MA (2014) Analysis and control of cable-stayed bridges subject to seismic action. Struct Eng Int 24(1):27–36. https://doi.org/10.2749/101686614x13830790993762
7. Camara A, Efthymiou E (2016) Deck–tower interaction in the transverse seismic response of cable-stayed bridges and optimum configurations. Eng Struct 124:494–506. https://doi.org/10.1016/j.engstruct.2016.06.017
8. Chang K-C, Mo Y, Chen C, Lai L, Chou C (2004) Lessons learned from the damaged Chi-Lu cable-stayed bridge. J Bridge Eng 9(4):343–352. https://doi.org/10.1061/(asce)1084-0702(2004)9:4(343)
9. Cen E (2004) 8—Design of structures for earthquake resistance—Part 1: General rules, seismic actions and rules for building. Br. Stand. Institute, London
10. CEN E (2004) 8—Design of structures for earthquake resistance—Part 2: Bridges. Br. Stand. Institute, London
11. Egyptian Code of Practice 207 for Planning, Design & Construction of Bridges & elevated intersections-part 4: forces and loads on bridges. Arab republic of egypt ministry of housing, utilities and urban development, (2015)
12. Egyptian Code of Practice 207 for Planning, Design & Construction of Bridges & elevated intersections-part 5: analyzing and design concrete bridges. Arab republic of egypt ministry of housing, utilities and urban development, (2015).
13. Greco F, Lonetti P, Pascuzzo A (2013) Dynamic analysis of cable-stayed bridges affected by accidental failure mechanisms under moving loads. Math Probl Eng 2013:1–20. https://doi.org/10.1155/2013/302706
14. Hambly EC (1991) Bridge deck behaviour, 2nd edn. Spon Press, London
15. Hariri B (2018) Resonance of Cable-Stayed Bridges Subjected to Delayed Time-Histories Using Multi-Support Excitation, MSc. (Master of Applied Science (Civil Engineering explanatory), Concordia University, Montreal, Quebec, Canada, pp 30–105
16. Hariri B, Lin L (2018) Evaluating the response of cable-stayed bridges subjected to delayed seismic time-histories using multi-support excitation. In: Paper presented at the Proceedings of the 3rd International Conference on Civil, Structural and Transportation Engineering (ICCSTE'18) Niagara Falls, Canada
17. Hua C-H, Wang Y-C (1996) Three-dimensional modeling of a cable-stayed bridge for dynamic analysis. In: Paper presented at the Proceedings of The 14th International Modal Analysis Conference
18. Kajita T, Cheung YJ (1973) Finite element analysis of cable-stayed bridges. IABSE Publ 33(11):101–112
19. Karoumi R (1999) Some modeling aspects in the nonlinear finite element analysis of cable supported bridges. Comput Struct 71(4):397–412
20. Karoumi R (2000) Modeling of cable-stayed bridges for analysis of traffic induced vibrations. In: Paper presented at the Proc., IMAC-XVIII Conf. on Structural Dynamics
21. Krishna P, Arya A, Agrawal TJ (1985) Effect of cable stiffness on cable-stayed bridges. J Struct Eng 111(9):2008–2020
22. Kunde M, Jangid R (2003) Seismic behavior of isolated bridges: A-state-of-the-art review. Electron J Struct Eng 3(2):140–169
23. Leonhardt F, Zellner W (1980) Cable-stayed bridges. IABSE Survey, AIPC Review, IVBH Berichte, 80(P-13/80)
24. Lonetti P, Pascuzzo A (2014a) Design analysis of the optimum configuration of self-anchored cable-stayed suspension bridges. Struct Eng Mech: Int J 51(5):847–866
25. Lonetti P, Pascuzzo A (2014b) Vulnerability and failure analysis of hybrid cable-stayed suspension bridges subjected to damage mechanisms. Eng Failure Anal 45:470–495
26. Niyitegeka S (2016) To Study the effect of Pylon Shapes on static and Dynamic Response of cable-stayed bridges, MSc. (Master of Engineering Degree in Civil - Structural Engineering explanatory), Marwadi Education Foundation Group of Institutions, Rajkot, Gujarat, India, (107) p 30-42

27. Poddar K, Rahman DT (2015) Comparative study of cable stayed, suspension and composite bridge. Int J Innov Res Sci, Eng Technol 4(9):8530–40
28. Podolny W Jr, Scalzi J (1986) Construction and design of cable-stayed bridges. Wiley, New York
29. Sarhang Zadeh, O. (2012). Comparison between three types of cable stayed bridges using structural optimization, MSc. (Master of Engineering Science explanatory), The University of Western Ontario, (116)
30. Shah DN, Desai DJ, Patil DH (2011) Effect of pylon shape on analysis of cable-stayed bridges. J Eng Res Stud 2(1):104–109
31. Smith B (1968) A Linear Method of Analysis for Double-Plane Cable-Stayed Girder Bridges. Proc Inst Civil Eng 39(JAN):85–125. https://doi.org/10.1680/iicep.1968.32692
32. Soneji B, Jangid R (2006) Effectiveness of seismic isolation for cable-stayed bridges. Int J Struct Stabil Dyn 6(01):77–96
33. Thakkar SP (2000) Parametric Study of Shapes of Pylon for Cable Stayed Bridge. Nirma Univ J Eng Technol 2(1):9–16
34. Wang P, Tseng T, Yang C (1993) Initial shape of cable-stayed bridges. Comput Struct 47(1):111–123
35. Wesolowsky MJ, Wilson JC (2003) Seismic isolation of cable-stayed bridges for near-field ground motions. Earthquake Eng Struct Dyn 32(13):2107–2126
36. Wilson JC, Gravelle W (1991) Modelling of a cable-stayed bridge for dynamic analysis. Earthquake Eng Struct Dyn 20(8):707–721. https://doi.org/10.1002/eqe.4290200802
37. Wilson JC, Liu T (1991) Ambient vibration measurements on a cable-stayed bridge. Earthquake Eng Struct Dyn 20(8):723–747. https://doi.org/10.1002/eqe.4290200803
38. Xu L (2014) Wind effects on cable-supported bridges: Xu/wind effects on cable-supported bridges, 1st edn. Wiley, Nashville

Publisher's Note